

Singlet levels of the NV⁻ centre in diamond

This content has been downloaded from IOPscience. Please scroll down to see the full text.

2015 New J. Phys. 17 013048

(<http://iopscience.iop.org/1367-2630/17/1/013048>)

View [the table of contents for this issue](#), or go to the [journal homepage](#) for more

Download details:

IP Address: 130.56.106.42

This content was downloaded on 19/05/2015 at 02:20

Please note that [terms and conditions apply](#).



PAPER

Singlet levels of the NV⁻ centre in diamond

OPEN ACCESS

RECEIVED
4 July 2014REVISED
7 November 2014ACCEPTED FOR PUBLICATION
8 December 2014PUBLISHED
27 January 2015Content from this work
may be used under the
terms of the [Creative
Commons Attribution 3.0
licence](#).Any further distribution of
this work must maintain
attribution to the author
(s) and the title of the
work, journal citation and
DOI.L J Rogers^{1,2,4}, M W Doherty¹, M S J Barson¹, S Onoda³, T Ohshima³ and N B Manson¹¹ Laser Physics Centre, Research School of Physics and Engineering, Australian National University, Canberra, ACT 0200, Australia² School of Science and Mathematics, Avondale College of Higher Education, Cooranbong, NSW 2265, Australia³ Semiconductor Analysis and Radiation Effects Group, Japan Atomic Energy Agency, 1233 Watanuki, Takasaki, Gunma 370-1292, Japan⁴ Current address: Institut für Quantenoptik, Universität Ulm, D-89081 Ulm, GermanyE-mail: lachlan.j.rogers@quantum.diamonds

Keywords: nitrogen-vacancy, diamond, uniaxial stress, infrared emission, spin polarization, colour centre

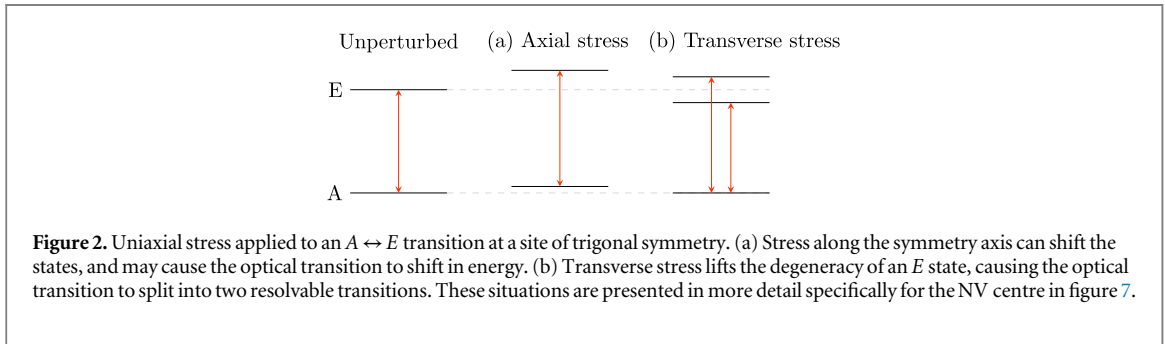
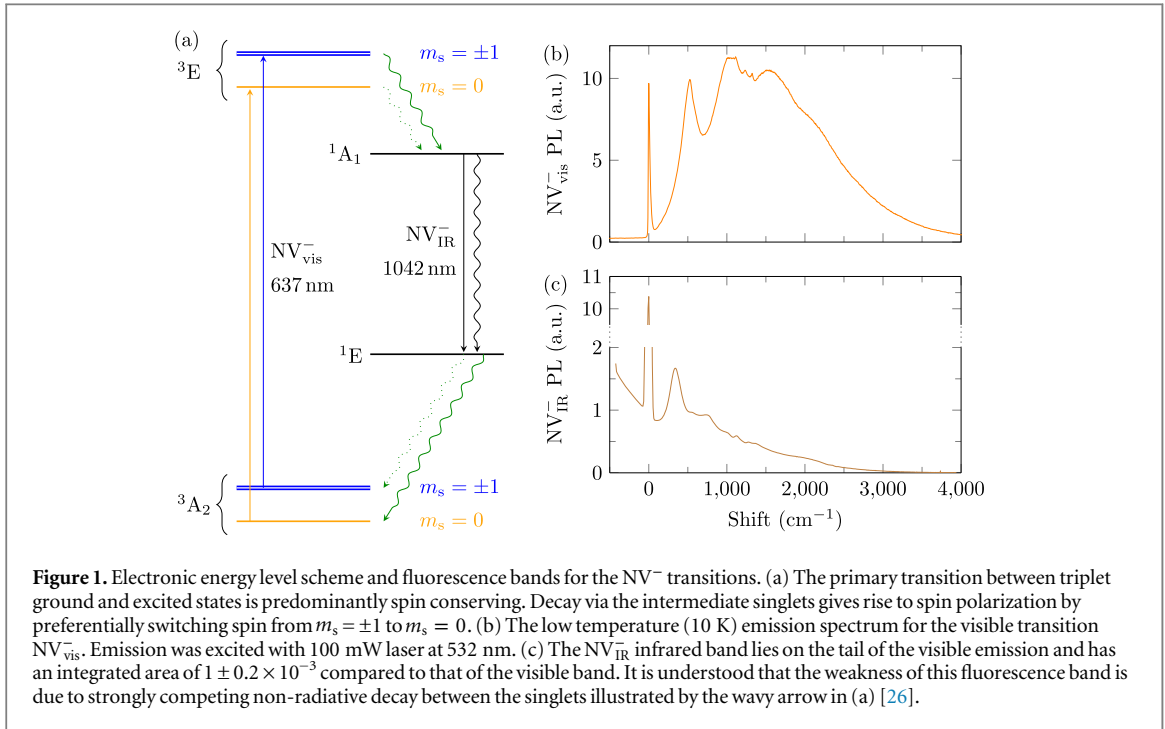
Abstract

The characteristic transition of the NV⁻ centre at 637 nm is between ³A₂ and ³E triplet states. There are also intermediate ¹A₁ and ¹E singlet states, and the infrared transition at 1042 nm between these singlets is studied here using uniaxial stress. The stress shift and splitting parameters are determined, and the physical interaction giving rise to the parameters is considered within the accepted electronic model of the centre. It is established that this interaction for the infrared transition is due to a modification of electron–electron Coulomb repulsion interaction. This is in contrast to the visible 637 nm transition where shifts and splittings arise from modification to the one-electron Coulomb interaction. It is also established that a dynamic Jahn–Teller interaction is associated with the singlet ¹E state, which gives rise to a vibronic level 115 cm⁻¹ above the ¹E electronic state. Arguments associated with this level are used to provide experimental confirmation that the ¹A₁ is the upper singlet level and ¹E is the lower singlet level.

1. Introduction

The negatively charged nitrogen vacancy centre in diamond (NV⁻) [1] exhibits optically induced spin polarization. This property underpins many exciting applications of the NV⁻ centre in fields such as magnetic sensing [2–9], biological imaging [10–12], and quantum information processing [13–17]. The principle zero-phonon line (ZPL) associated with the centre is at 637 nm (1.945 eV, 15687 cm⁻¹) and is found by uniaxial stress to involve a transition between a ground state of A symmetry and an excited state of E symmetry at a trigonal site [18]. Here we label this transition NV⁻_{vis} since it is in the visible spectrum, and its fluorescence band is shown in figure 1. The ground and excited states are spin triplets [19–23] and optical excitation of this transition results in the spin being polarized into m_s = 0, although this does not arise from direct optical cycling as the optical transitions are spin-conserving [24]. When the triplet system is excited there is also relaxation via intermediate singlets and this decay causes the spin polarization. A weak emission band in the infrared (figure 1) with a ZPL at 1042 nm (1.19 eV, 9597 cm⁻¹) is associated with decay between these two singlet levels [25].

A study of this emission (which we call NV⁻_{IR}) provides an opportunity to better understand the electronic levels in this important decay channel. Uniaxial stress is the experimental technique of choice [27–29]. In these experiments external stress close to the limits of fraction is applied to the diamond along well-defined crystal axes while the displacement and splitting of the ZPL are measured. The precise effects depend on the orientation of the impurity centre relative to the stress axis, and provide information about the orbital symmetry of the states involved with optical transitions. A previous uniaxial stress study has shown that the NV⁻_{IR} transition is between levels of A and E symmetry [25], and this symmetry assignment is not in question. However, in that study the specific transitions were not correctly identified and this led to an inaccuracy of the stated stress parameters. Here the transitions are unambiguously identified and correct stress parameters are determined. In addition we experimentally resolve the long-standing contention regarding the order of the singlets [25, 30–33] and establish the ¹E to be the lower singlet. The magnitudes of the stress parameters are considered within the current



electronic model of the centre. It is concluded that the interaction giving rise to the shift and splitting of the infrared ZPL is different from that giving rise to the shifts and splittings of the NV_{vis}^- ZPL and NV^0 ZPL.

2. Uniaxial stress theory

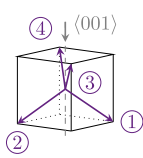
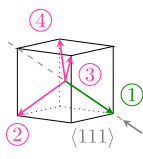
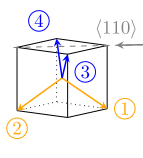
The theory for uniaxial stress applied to an $A \leftrightarrow E$ transition at a site of trigonal symmetry in a cubic crystal has been given on several occasions [27–29, 34] and has been developed by Davies and Hamer [18, 35] for the case of the NV centre. In general, stress along the symmetry axis results in shifts of the energy levels while transverse stress lifts the degeneracy of the E state as illustrated in figure 2. The elements of the stress tensor s_{ij} as applied to the cubic crystal can be expressed in terms of the irreducible representations appropriate for the trigonal site symmetry, and the stress perturbation at the NV site is given by

$$\begin{aligned}
 H^s = & A_1 (s_{xx} + s_{yy} + s_{zz}) + A_1' (s_{yz} + s_{zx} + s_{xy}) \\
 & + E_X (s_{xx} + s_{yy} - 2s_{zz}) + E_Y \sqrt{3} (s_{xx} - s_{yy}) \\
 & + E_X' (s_{yz} + s_{zx} - 2s_{xy}) + E_Y' \sqrt{3} (s_{yz} - s_{zx}),
 \end{aligned} \quad (1)$$

where A_1, A_1' are symmetry adapted electronic operators transforming as A_1 irreducible representations and E_X, E_Y, E_X', E_Y' are operators transforming as components of E irreducible representations [18, 29]. The stress s_{ij} is given in terms of the lattice co-ordinates. The effects of this interaction on an $A \leftrightarrow E$ transition have been described by Davies and Hamer [18] in terms of the following reduced matrix elements

$$A_1 = \langle E \| A_1 \| E \rangle - \langle A \| A_1 \| A \rangle, \quad (2)$$

Table 1. Summary of shifts, splittings and polarization for stress applied along several crystallographic directions. The values are from reference [18] although here the values are normalized to an intensity of 8/3 at zero stress (each of the four orientations contributing a relative oscillator strength of two). Intensities are given for π (electric field vector parallel to stress) and σ (perpendicular) polarizations. The selection rules were given for $A_1 \leftrightarrow E$ transitions [18] and are extended here to also cover $A_2 \leftrightarrow E$ transitions. The change results in an interchange of X and Y and change of sign of B and C .

Stress	Orientation	Sym	E state Energy	$A_2 \leftrightarrow E$		$A_1 \leftrightarrow E$		
				π	σ	π	σ	
	①							
	② 54° (XZ)	$E_X (I_1)$	$A_1 + 2B$	0	2	$\frac{8}{3}$	$\frac{2}{3}$	
	③							
	④	$E_Y (I_2)$	$A_1 - 2B$	$\frac{8}{3}$	$\frac{2}{3}$	0	2	
	① 0°	E_X, E_Y	$A_1 + 2A_2$	0	1	0	1	
	②							
	③ 70° (XZ)	$E_X (I_1)$	$A_1 - \frac{2}{3}A_2 + \frac{4}{3}C$	0	$\frac{3}{2}$	$\frac{8}{3}$	$\frac{1}{6}$	
	④	$E_Y (I_2)$	$A_1 - \frac{2}{3}A_2 - \frac{4}{3}C$	$\frac{8}{3}$	$\frac{1}{6}$	0	$\frac{3}{2}$	
	① 36° (XZ)	$E_X (I_1)$	$A_1 + A_2 - B + C$	σ_{110}	σ_{001}	σ_{110}	σ_{001}	
	②	$E_Y (I_2)$	$A_1 + A_2 + B - C$	0	2	0	2	$\frac{4}{3}$
	③ 90° (YZ)	$E_X (I_1)$	$A_1 - A_2 - B - C$	$\frac{2}{3}$	0	$\frac{4}{3}$	0	$\frac{4}{3}$
	④	$E_Y (I_2)$	$A_1 - A_2 + B + C$	0	$\frac{2}{3}$	$\frac{4}{3}$	2	0

$$2A_2 = \langle E \| A'_1 \| E \rangle - \langle A \| A'_1 \| A \rangle, \quad (3)$$

$$\sqrt{2}B = \langle E \| E \| E \rangle, \quad (4)$$

$$\sqrt{2}C = \langle E \| E' \| E \rangle. \quad (5)$$

For stress applied along $\langle 001 \rangle$, $\langle 111 \rangle$ and $\langle 110 \rangle$ crystallographic directions, the resultant relative strength and polarization of the transitions have been given in previous publications [18, 27–29, 34] and are summarized in table 1. Since the NV centre is now known to involve both $A_1 \leftrightarrow E$ and $A_2 \leftrightarrow E$ transitions as indicated in figure 1 the selection rules for both cases have been included in table 1. Stress along $\langle 001 \rangle$, $\langle 111 \rangle$ or $\langle 110 \rangle$ directions is always in a reflection plane or at right angles to a reflection plane, and consequently the site symmetry is always lowered to C_s . Therefore, for every case the I_1 or I_2 irreducible representations for C_s are included in the table.

3. Experimental details

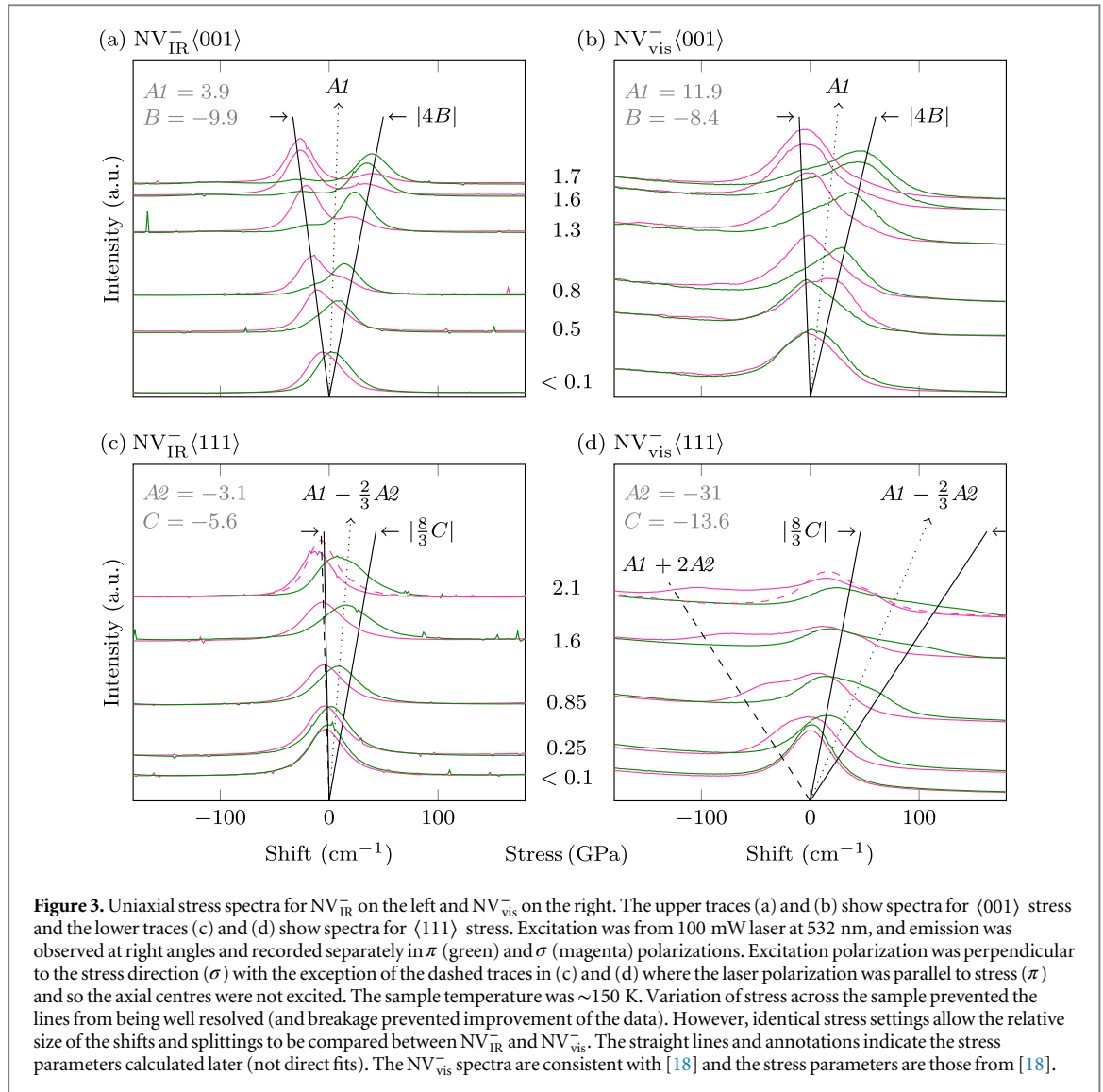
Diamond cubes with dimensions $2 \times 2 \times 2$ mm were used. They have nitrogen concentrations of ~ 100 ppm and were irradiated and annealed to give NV^- concentrations of ~ 5 ppm. The cubes had either $\langle 110 \rangle$, $\langle 1\bar{1}0 \rangle$ and $\langle 001 \rangle$ faces or $\langle 111 \rangle$, $\langle 1\bar{1}0 \rangle$ and $\langle 11\bar{2} \rangle$ faces. These were used for application of stress along $\langle 001 \rangle$, $\langle 111 \rangle$ and $\langle 110 \rangle$ directions by means of a pneumatic driven rod. The samples were within a cryostat and could be cooled to liquid helium or liquid nitrogen temperatures as required.

For the majority of the work the emission was excited by a laser at a wavelength of 532 nm within the vibrational sideband of the ${}^3A_2 \rightarrow {}^3E$ absorption transition. The emission at right angles was dispersed by a monochromator and detected by a photomultiplier (for NV_{vis}^-) or a cooled germanium detector (for NV_{IR}^-). A tunable dye laser at the wavelength of the visible ZPL was used for selective excitation techniques to assist with the assignments of the NV_{IR}^- spectra.

4. Results

4.1. Uniaxial stress measurements along $\langle 001 \rangle$ and $\langle 111 \rangle$

Although both the visible [18] and infrared [25] transitions involve an $A \leftrightarrow E$ transition at a site of trigonal symmetry, NV_{vis}^- involves an A_2 state whereas NV_{IR}^- involves an A_1 . In addition, the E state is the upper level for



NV_{vis}^- but for NV_{IR}^- the E is the lower level (proven later). These two differences cancel to result in the same stress patterns for the NV_{vis}^- and NV_{IR}^- transitions. Conveniently this allows the visible and infrared spectra to be easily compared to obtain the relative magnitudes of the NV_{vis}^- and NV_{IR}^- stress parameters. This is the intention of presenting figure 3 where spectra of NV_{vis}^- and NV_{IR}^- are depicted for the same stress applied along the $\langle 001 \rangle$ and $\langle 111 \rangle$ directions.

For stress along $\langle 001 \rangle$ the splittings are the same for all orientations of the NV^- centre. The ZPL is split into two components with one component σ polarized (electric field vector perpendicular to stress) and the other predominantly π polarized (parallel to stress). The splittings are determined by the value of the B parameter (see table 1) and the average shift is given by $A1$. It can be seen from comparing figures 3(a) and (b) that B_{IR} is marginally larger than B_{vis} whereas $A1_{IR}$ is only about one third of $A1_{vis}$.

For $\langle 111 \rangle$ stress there are two subsets of centres (table 1). One subset contains the centres oriented along the stress direction, for which there is no change of symmetry. This means there is no splitting, but the transition is shifted by $A1 + A2$ (table 1). NV^- centres in this orientation are not excited when the electric field vector of the excitation is parallel to their axis, since the $A \leftrightarrow E$ transitions do not involve a z dipole moment. Consequently this orientation does not contribute to the dashed traces of figures 3 (c) and (d) where this excitation polarization is adopted. The NV^- centres in this orientation do give a line when transverse excitation is used. This ‘extra’ line is barely discernible in the case of the infrared spectrum as it overlaps the other features indicating a very small shift ($A1_{IR} + A2_{IR}$). In contrast, there is a large shift of this line for the visible transition. Since $A1_{vis}$ and $A1_{IR}$ are known from the above $\langle 001 \rangle$ stress measurements, it can be readily deduced that $A2_{vis}$ for the visible is large and negative whereas $A2_{IR}$ for the infrared is small. This information is consistent with average shifts for the centres oriented at 70° to the $\langle 111 \rangle$ stress given by $A1 + \frac{2}{3}A2$ (table 2). The ZPL splitting for these centres depends on the C parameter, and it is apparent that C_{IR} is about one third of C_{vis} .

Table 2. Stress parameters of the NV_{IR}^- ZPL compared to those for NV_{vis}^- , NV^0 and N3, given in $cm^{-1} GPa^{-1}$ ($meV GPa^{-1}$). These are all $A \leftrightarrow E$ transitions at trigonal vacancy centres with adjacent nitrogen atoms. The values for NV_{vis}^- are taken from [18] although B and C sign change is appropriate for the $A_2 \leftrightarrow E$ transition. Uncertainty estimates for the ratios were calculated assuming a 7% uncertainty in the NV_{vis}^- parameters from [18]. The values for NV^0 are from [35] and N3 from [34].

	NV_{IR}^- 1042.6 nm	NV_{vis}^- 637 nm	NV_{IR}^-/NV_{vis}^- ratio	NV^0 575 nm	N3 415 nm
Param (pert)	$cm^{-1}(meV)$	$cm^{-1}(meV)$		$cm^{-1}(meV)$	$cm^{-1}(meV)$
$A1 (A_1)$	$3.9 \pm 0.3 (0.48)$	$11.9 (1.47)$	0.33 ± 0.05	$8.5 (1.05)$	$4.0 (0.5)$
$A2 (A_1')$	$-3.1 \pm 0.3 (-0.38)$	$-31.0 (-3.85)$	0.10 ± 0.02	$-28.6 (-3.55)$	$34 (4.2)$
$B (E)$	$-9.9 \pm 0.5 (-1.23)$	$-8.38 (-1.04)$	1.2 ± 0.1	$12.5 (1.55)$	$-8.5 (-1.55)$
$C (E')$	$-5.6 \pm 0.5 (-0.69)$	$-13.6 (-1.69)$	0.41 ± 0.07	$14.1 (1.76)$	$-11 (-1.9)$

The conclusion that $A1_{IR}$ and $C1_{IR}$ are a factor of three smaller than their NV_{vis}^- counterparts is consistent with the NV_{IR}^- strain parameters reported previously [25]. However, there is no consistency with the $A2_{IR}$ and $B1_{IR}$ parameters. Here we have established that $A2_{IR}$ is an order of magnitude smaller than $A2_{vis}$ (instead of the factor of 2.7 given previously), and that $|B1_{IR}| > |B1_{vis}|$ (instead of the reverse). The previous values relied on the interpretation of spectra for stress along the $\langle 110 \rangle$ direction and, therefore, the spectra for this stress direction are re-investigated in the next section.

4.2. Uniaxial stress along $\langle 110 \rangle$ stress using selective excitation

Stress along $\langle 110 \rangle$ causes the NV^- centres to form two distinct sets of orientations, both of which have some component of transverse strain and therefore exhibit splitting (table 1). This produces a four-line structure in the spectrum, and the determination of strain parameters depends heavily on a correct assignment of each line to a transition in a given NV orientation. Here we use selective excitation techniques to provide reliable assignments.

A 200 mW tunable dye laser was swept through the NV_{vis}^- ZPL and the emission was detected in the vibronic sideband between 650 nm and 750 nm. Weak (1 mW) 532 nm laser light was applied simultaneously to inhibit loss of signal through hole burning. The polarized NV_{vis}^- excitation spectra for a $\langle 110 \rangle$ stress of 1.4 GPa obtained in this way is shown in figure 4(a). This NV_{vis}^- excitation spectrum is consistent with the measurements of Davies and Hamer obtained in absorption [18]. The two higher energy lines in excitation (at 632.4 nm and 634.8 nm) are associated with centres at right angles to the stress (orientations ③ and ④, table 1), and the lower energy NV_{vis}^- lines are associated with orientations ① and ② which are at 36° to the stress [18].

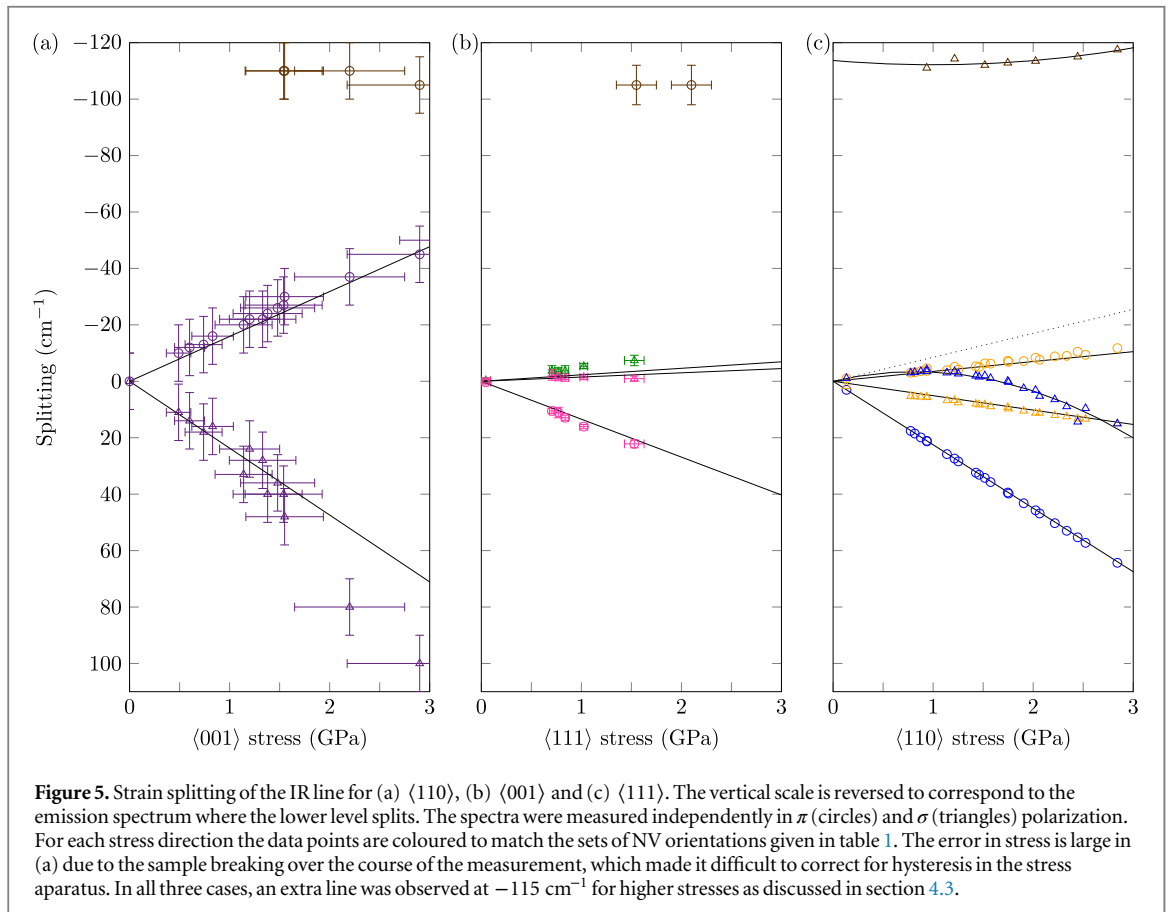
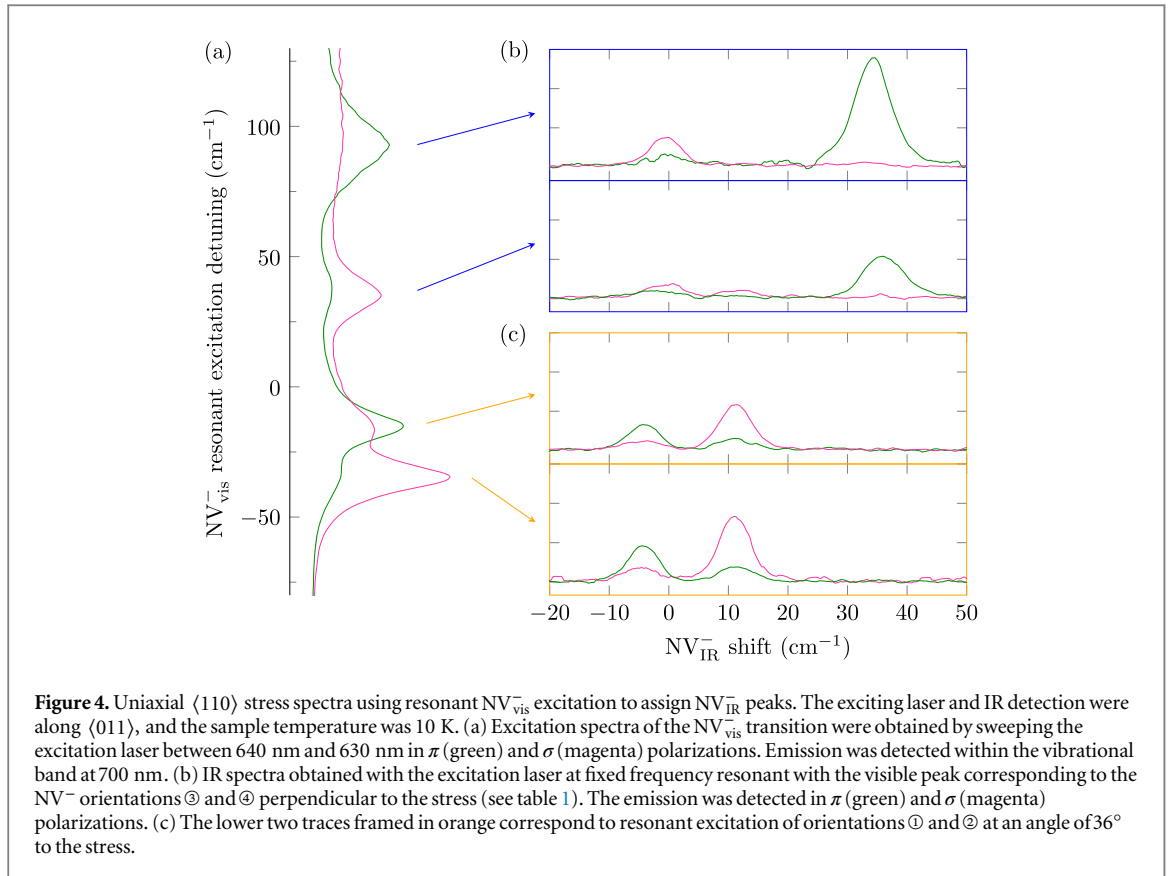
The detection filter was changed to measure emission in the NV_{IR}^- band. Resonantly exciting the two higher energy NV_{vis}^- transitions gave the polarized NV_{IR}^- spectra shown in figure 4(b). Since these laser frequencies only excite the orientations ③ and ④ which are orthogonal to the stress, the NV_{IR}^- spectrum shows only two lines. These lines are clearly either predominantly π or σ polarized, enabling them to be assigned to the I_1 and I_2 components according to table 1. Tuning the laser to the lower energy NV_{vis}^- transitions caused only orientations ① and ② to be excited, producing the NV_{IR}^- spectra shown in figure 4(c). Again the lines are strongly polarized and readily assigned using table 1. There is always the equivalence between the visible and infrared spectra described in previous section but it is noted that the order of the π and σ lines for the 36° case are reversed between the visible and infrared spectra. This results from a reversal of the relative strengths of the B and C stress parameters between the visible and infrared cases with $B_{IR} > C_{IR}$ in one case and $C_{vis} > B_{vis}$ in the other.

These selective excitation measurements provide the first unambiguous assignments of the infrared spectral features for $\langle 110 \rangle$ stress. It is now clear that the significantly different $A2_{IR}$ and $B1_{IR}$ splitting parameters given previously [25] resulted from an incorrect assignment of the NV_{IR}^- lines for $\langle 110 \rangle$ stress. In that work it was assumed that the four peaks were in the same order as for NV_{vis}^- , which does not turn out to be the case.

Having established the identity of each line in the spectrum, more conventional photoluminescence measurements were made using the 532 nm non-resonant excitation. In this way the position of the four lines in the stress spectra were followed for stress values in the range 0–3 GPa, and the shifts and splittings are shown in figure 5. This figure also includes the results for stress along $\langle 001 \rangle$ and $\langle 111 \rangle$, where there is less ambiguity in the assignments of the lines and therefore no advantage to adopting selective excitation techniques. It can be seen from the figures that the displacements with stress are not always linear and this requires consideration before the values of the stress parameters can be deduced.

4.3. High stress and extra feature at $115 cm^{-1}$

At higher stress (>1 GPa) an extra feature was found to be induced $115 \pm 5 cm^{-1}$ to the low energy side of the ZPL. Its position is indicated in figures 5 and 6 shows spectra exhibiting this peak for $\langle 111 \rangle$, $\langle 110 \rangle$, and $\langle 001 \rangle$



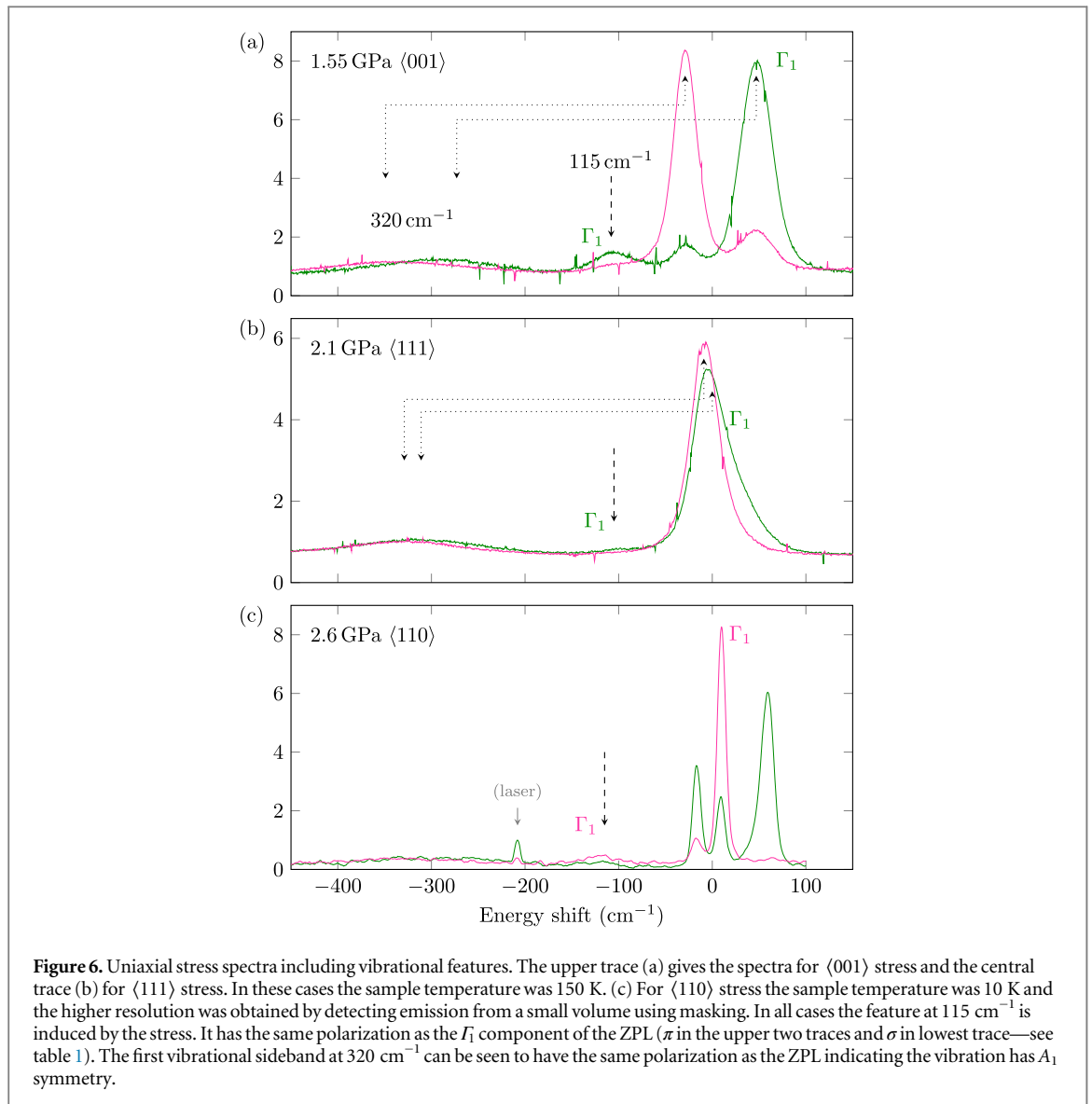


Figure 6. Uniaxial stress spectra including vibrational features. The upper trace (a) gives the spectra for $\langle 001 \rangle$ stress and the central trace (b) for $\langle 111 \rangle$ stress. In these cases the sample temperature was 150 K. (c) For $\langle 110 \rangle$ stress the sample temperature was 10 K and the higher resolution was obtained by detecting emission from a small volume using masking. In all cases the feature at 115 cm^{-1} is induced by the stress. It has the same polarization as the Γ_1 component of the ZPL (π in the upper two traces and σ in lowest trace—see table 1). The first vibrational sideband at 320 cm^{-1} can be seen to have the same polarization as the ZPL indicating the vibration has A_1 symmetry.

stress. The feature appears with varying intensities but increases in strength with stress at the expense of a component of the ZPL with the same polarization. The measurements were made at higher resolution for the case of $\langle 110 \rangle$ uniaxial stress, and it is apparent that the extra feature gains at the expense of the line displaced nonlinearly. It also shifts slightly in the reverse direction, as shown in figure 5(c). This is typical for a situation where there are two interacting levels which have the same symmetry. From the analysis of the ZPL it has been established that the line shifting nonlinearly has Γ_1 in C_s symmetry. The extra feature will, therefore, also have Γ_1 in C_s and since it is not split it must have A_1 symmetry in C_{3v} .

This symmetry assignment is consistent with its occurrence for other stress directions. For $\langle 001 \rangle$ stress the line displaced to higher energy has π polarization and is assigned to a Γ_1 state, and this line mixes with the extra feature (figure 6(a)). Even though the interacting ZPL component is shifting away from the 115 cm^{-1} feature, the displacement of this ZPL line becomes nonlinear as a result of the interaction, as shown in figure 5(a). Here it might be expected that the 115 cm^{-1} feature shifts in the reverse direction, but the effect is reduced owing to the proximity of the 320 cm^{-1} vibrational level. Indeed at the highest stress it is observed that there is a slight shift of the extra feature to shorter wavelength (higher energy) owing to the latter interaction. In the third case of $\langle 111 \rangle$ the effects are small but the feature again has the same polarization as that for the Γ_1 component of the split ZPL (figure 6(b)).

Since the 115 cm^{-1} feature interacts with one component of a line that splits with stress, it must be associated with the 1E electronic state. It occurs on the low energy side of the ZPL in the emission spectrum. Should the 1E be the upper singlet level there will be relaxation to this level 115 cm^{-1} below the 1E state and at cryogenic temperatures ($<30 \text{ K}$) all the emission would be from this level. This is not the case and it is concluded that the 1E is not the upper singlet level. The alternative is that the 1E is the lower singlet level and the extra level lies

115 cm⁻¹ above it. This confirms our previous report [36] and is consistent with the now generally accepted theoretical model [37, 38].

The occurrence of low-energy vibronic levels in diamond is a fairly common observation and has been observed in previous uniaxial stress studies of diamond [35]. They are associated with a dynamic Jahn–Teller effect associated with an E state. Davies [35] has established five other cases of trigonal centres in diamond exhibiting this effect. The first vibrational state associated with a degenerate E vibration will involve the electronic and the vibration states, resulting in four vibronic states with symmetries $E \times E = A_1 + A_2 + E$. The E vibronic level is displaced up in energy and the $A_1 + A_2$ down. Quadratic electron-vibration interaction will lift the A_1 and A_2 degeneracy and result in the low lying A_1 state at 115 cm⁻¹ as observed here. A similar situation arises in the case of the 2E ground state of NV⁰ [35]. In this case the level occurs at 110 cm⁻¹ and from the similarity in the situation it can be expected that the strength of the Jahn–Teller interaction is similar: $E_{JT}/\hbar\omega \sim 2$.

This vibronic level has significant implications. It has been used above to establish the order of the singlet levels, resolving long-standing contention about this detail of the NV electronic structure [25, 30–33]. It should also be noted that one consequence of the dynamic Jahn–Teller interaction is a reduction of the effect of perturbations [39]. Thus the experimental measurements of the stress splittings will be slightly smaller than obtained from calculation unless such effects are included.

4.4. Stress parameters

The nonlinear shift of some spectral features with stress is, therefore, due to interaction with vibronic levels. Modelling these interactions is not straightforward as they can involve a distribution of vibrations and the distribution need not be simple. Consequently we have determined the stress parameters using shifts and splitting at levels of stress where the strength of this latter interaction is negligible, essentially using the asymptotic slopes at zero stress. The value of the parameters are given in table 2.

5. Discussion of the molecular model

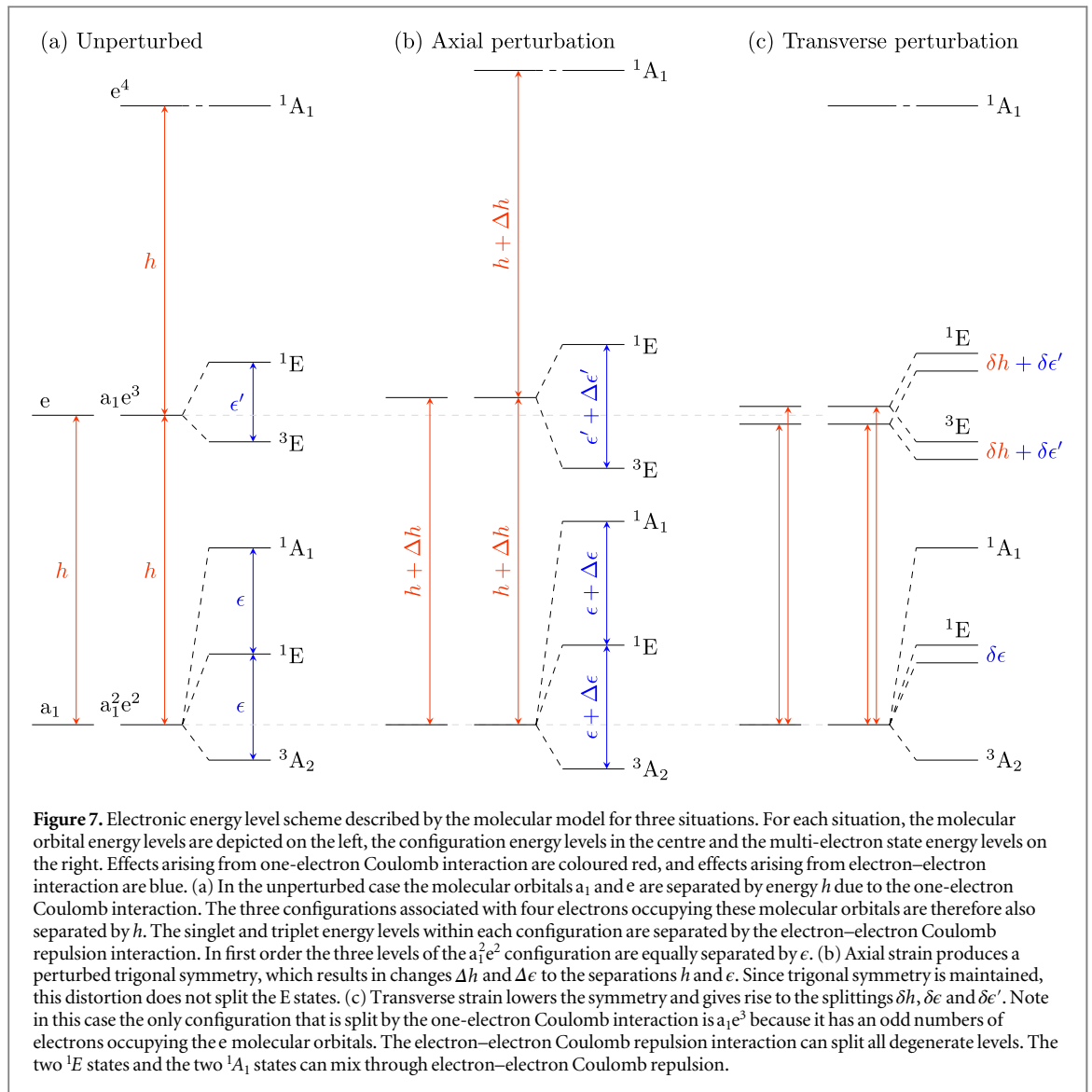
The electronic model of the NV⁻ centre has its foundations in the defect-molecule approach of Coulson and Kearsley [40] and has been given in detail by many authors [1, 32, 37, 38, 41]. The centre's electronic states are written in terms of symmetry-adapted molecular orbitals. There are four unbound sp³ atomic orbitals adjacent to the vacancy and in C_{3v} symmetry these can be linearly combined to give two degenerate orbitals that transform as the E irreducible representation (denoted as e-orbitals) and two separate orbitals of A₁ symmetry (denoted as a₁-orbitals). These are occupied by six electrons: one from each of the adjacent carbon atoms, two from the nitrogen, and one acquired from the lattice. The lower a₁ orbital is always occupied and need not be included in a description of the states. The occupancy of the other four electrons describe the multi-electron states.

The non-relativistic electronic Hamiltonian of the NV⁻ centre may be defined as [37]

$$H(\vec{r}, \vec{R}) = T_e(\vec{r}) + V_{Ne}(\vec{r}, \vec{R}) + V_{ee}(\vec{r}),$$

where T_e is the electronic kinetic energy, V_{Ne} is the one-electron Coulomb interaction between the NV electrons and the lattice nuclei and electrons, V_{ee} is the electron–electron Coulomb repulsion interaction of the NV electrons, \vec{r} are the collective coordinates of the NV electrons and \vec{R} are the collective coordinates of the lattice. Both T_e and V_{Ne} can be written as sums of one-electron operators, whereas V_{ee} can be written as a sum of two-electron operators. The molecular orbitals are defined as solutions of the one-electron terms $T_e + V_{Ne}$. The a₁ and e molecular orbitals have energies that lie within the diamond band gap and are separated by $h \sim 2$ eV (figure 7(a)). The energies of the a₁ and e molecular orbitals define the energies of the electronic configurations. The four electrons occupying these molecular orbitals lead to three configurations a₁²e², a₁e³ and e⁴, which are each separated by h (figure 7(a)). The introduction of the electron–electron Coulomb interaction V_{ee} separates the multi-electron states within a configuration into triplet and singlet levels. The separation can be of the order of eV and, hence, comparable in magnitude to that of the one-electron terms. For example, the lowest energy configuration a₁²e² is split into equally separated states 3A_2 , 1E and 1A_1 with separations of $e \sim 1$ eV [37, 38] (figure 7(a)). The electron–electron Coulomb repulsion interaction can also give interaction between configurations and mix the singlet levels of the same orbital symmetry, thereby modifying the simple expressions for ϵ and ϵ' .

The above one- and two-electron Coulomb interactions give the dominant terms in determining the effects of stress, which are observed to be several meV. Other electronic interactions such as spin–orbit and spin–spin are less than meV and their effects are negligible compared to stress. Whilst electron-vibration interaction can be of the order of meV, it can not give stress splitting by itself. Although, as mentioned earlier, it can modify the



magnitude of stress splittings in the case of dynamic Jahn–Teller interaction [39]. Hence, the analysis of the stress parameters can be largely restricted to consideration of the Coulomb interactions.

When stress is applied, the lattice coordinates \vec{R} change, which results in a change δV_{Ne} [s] of the one-electron Coulomb interaction that in turn modifies the molecular orbitals and their energies. Furthermore, the modification of the molecular orbitals occupied by the electrons leads to a change in the electron–electron Coulomb repulsion interaction, which can be represented by the effective operator δV_{ee} [s]. Note that δV_{Ne} [s] + δV_{ee} [s] can be expanded in symmetry adapted form with terms that are in one to one correlation with those in equation (1). If the symmetry is not changed by the applied stress, δV_{Ne} [s] will only alter the a_1 – e energy separation and this is denoted by Δh (figure 7(b)). This will result in a change of the energy separation between configurations but cause no change within each configuration (figure 7(b)). Where the applied stress lowers the symmetry of the centre, δV_{Ne} [s] will result in a splitting of the e molecular orbitals by δh . The consequence is that the multi-electron E states with an odd number of electrons occupying the e molecular orbitals will be split by δh (figure 7(c)). Significantly, no splitting occurs when an even number of electrons occupy the e molecular orbitals. For each pair of electrons, one of the e electrons is moved up in energy and the other down, such that there is no overall splitting.

It is convenient to first consider the δV_{Ne} [s] interaction in relation to the singlet transition. The ${}^1A_1(a_1^2e^2) \leftrightarrow {}^1E(a_1^2e^2)$ transition is between levels within the same $a_1^2e^2$ configuration and so the transition energy can not be shifted by δV_{Ne} [s]. In addition, the ${}^1E(a_1^2e^2)$ state has an even number of electrons occupying the e molecular orbitals and so there will be likewise no splitting arising from δV_{Ne} [s]. Mixing between NV_{IR}^- singlet levels and the singlet levels above the excited 3E state can change this situation for both the shift and splittings. The shift of NV_{IR}^- due to the δV_{Ne} [s] interaction is second order in the singlet level mixings, and should

be proportional to the shift of NV_{vis}^- . This would cause the $A1$ and $A2$ parameters to have the same ratio (equal to $\sim 2\kappa_A^2 - \kappa_E^2$, where κ_A and κ_E are the mixing coefficients of the A_1 and E singlet levels, respectively). Clearly this is in conflict with the observed $A1$ ratio of 0.33 and $A2$ ratio of 0.1 (table 2). Hence, the experimental shifts of the singlet transition can not be simply explained by the $\delta V_{\text{Ne}} [s]$ interaction. The splitting of NV_{IR}^- due to $\delta V_{\text{Ne}} [s]$ occurs at first order in κ_E . Thus, particularly given the previous conclusion, it is unlikely that $\delta V_{\text{Ne}} [s]$ is predominately responsible for the observation that splitting parameters B and C are of comparable size between NV_{vis}^- and NV_{IR}^- (table 2). The dominant interaction giving rise to the stress shift and splitting of the singlet transition at 1042 nm must result from an alternative interaction. The most obvious candidate, given the magnitude of this interaction, is electron–electron Coulomb repulsion interaction $\delta V_{\text{ee}} [s]$. The first order changes are taken to be $\Delta\epsilon$ and $\delta\epsilon$ for axial and transverse stress, respectively (figures 7(b) and (c)). Such perturbations can account for the change of the ${}^1A_1 (a_1^2e^2)$ to ${}^1E (a_1^2e^2)$ separation and the splitting of the ${}^1E (a_1^2e^2)$ level.

The situation for the ${}^3A_2 (a_1^2e^2) \leftrightarrow {}^3E (a_1e^3)$ triplet transition is very different. The transition is between states of different configuration and the ${}^3E (a_1e^3)$ state has an odd number of electrons occupying the e molecular orbitals. Consequently, the shifts and splitting of the NV_{vis}^- can arise as a consequence of the changes of the one-electron Coulomb interaction $\delta V_{\text{Ne}} [s]$. However, the possibility that there are contributions from $\delta V_{\text{ee}} [s]$ cannot immediately be eliminated. To determine how much this latter term contributes, it is worth considering the situation for NV^0 .

The NV^0 centre has one less electron and its transition is between a ${}^2E (a_1^2e)$ ground state and a ${}^2A_2 (a_1e^2)$ excited state [42]. This 2E ground state has an odd number of electrons occupying the e molecular orbitals and hence can be split as a result of the $\delta V_{\text{Ne}} [s]$ interaction. It is also the sole state of the a_1^2e configuration and so there can be no contribution from $\delta V_{\text{ee}} [s]$. Therefore, the splitting of the NV^0 ZPL at 575 nm must arise solely from the $\delta V_{\text{Ne}} [s]$ interaction. The splitting is that of a single e–electron and is expected to be of similar magnitude (but opposite sign) to that of the single e–hole in the case of ${}^3E (a_1e^3)$. From table 2 it is clear that the B and C parameters have similar magnitude for NV_{vis}^- and NV^0 , which is consistent with this expectation. This provides strong evidence that the dominant contribution to the splitting of the NV_{vis}^- transition arises from the $\delta V_{\text{Ne}} [s]$ interaction, and any contribution from $\delta V_{\text{ee}} [s]$ is minor.

The NV^- centre is the first colour centre in diamond where the stress parameters are known for two separate transitions, and this provides an ideal situation for testing theoretical calculations. For example it may help determine whether the separate contributions from one-electron Coulomb interaction and electron–electron Coulomb repulsion interaction, as outlined above, can be justified. Having similar information for a transition in the closely related neutral charge state NV^0 [35] is also valuable. The N3 centre is another nitrogen-related colour centre that has been studied by uniaxial stress [34]. It involves three nitrogen atoms and one carbon adjacent to a vacancy, rather than the three carbon and one nitrogen, and a similar molecular model is adopted for describing its electronic states. Despite the stress parameters being similar to those of NV_{vis}^- , in this case the molecular model has not successfully predicted all of the excited states [43]. Having the stress parameters for four related transitions as given in table 2 provides valuable information for *ab initio* calculations to test our understanding of the electronic model of nitrogen-related colour centres in diamond.

6. Summary and conclusions

The aim of the work was to use uniaxial stress techniques to better understand the singlet levels of the nitrogen–vacancy centre in diamond. The 1042 nm ZPL is understood to be associated with the singlet to singlet transition between levels in the same configuration. The ZPL is spectrally narrow, the sideband is weak, and the symmetry maintaining stress shift parameters $A1$ and $A2$ are also relatively small and these are all characteristics of a transition between levels in the same electronic configuration. The ${}^1A_1 (a_1^2e^2) \leftrightarrow {}^1E (a_1^2e^2)$ singlet–singlet transition is the only transition within the electronic model that satisfies this condition and these aspects all give confidence that the transition is correctly identified. However, the stress splitting parameters are large and comparable with those for the $A \leftrightarrow E$ triplet and doublet transitions of NV_{vis}^- and NV^0 , respectively. These latter transitions involve a change of configuration and an E state with an odd number of e electrons. Consequently, one-electron Coulomb interaction can account for such effects. The singlet–singlet transition is different since the one-electron Coulomb interaction can not (in first order) split or shift the ZPL, and so it was anticipated the responses would be smaller. The strain parameters for NV_{IR}^- must arise from an alternative interaction and in this work it has been shown that they can be attributed to the two-electron Coulomb repulsion term. It is recognized within the Coulson and Kearsley [40] model that Coulomb repulsion always plays a significant role and in the case of the NV^- centre this interaction is of comparable magnitude to the one-electron Coulomb term. It is, therefore, realistic that the one-electron and two-electron Coulomb interactions can result in similar energy changes in response to a distortion of the lattice. The conclusion is that there is overall consistency with

the current electronic model of the NV⁻ and it follows that there is an adequate understanding of the singlet states.

The present uniaxial stress studies have also established that there is a dynamic Jahn–Teller effect associated with the ¹E level. Combining this observation with previous reports of dynamic Jahn–Teller effect in the excited ³E state, it is clear that electron–vibration interaction is significant within the NV⁻ system. The presence of electron–vibration interaction has been determined from observations within the ¹E and ³E degenerate electronic states independently, but the interaction can have more significant consequences between states. In particular, it can play a role in inter-system crossing between ³E and ¹A₁ and between ¹E and ³A₂ triplet and play a very important role in giving rise to the important spin polarization property of NV⁻.

Acknowledgments

This work was supported by the Australian Research Council (DP 120102232).

References

- [1] Doherty M W, Manson N B, Delaney P, Jelezko F, Wrachtrup J and Hollenberg L C L 2013 The nitrogen-vacancy colour centre in diamond *Phys. Rep.* **528** 1–45
- [2] Chernobrod B M and Berman G P 2005 Spin microscope based on optically detected magnetic resonance *J. Appl. Phys.* **97** 014903
- [3] Degen C L 2008 Scanning magnetic field microscope with a diamond single-spin sensor *Appl. Phys. Lett.* **92** 243111
- [4] Taylor J M, Cappellaro P, Childress L, Jiang L, Budker D, Hemmer P R, Yacoby A, Walsworth R and Lukin M D 2008 High-sensitivity diamond magnetometer with nanoscale resolution *Nat. Phys.* **4** 810–6
- [5] Maze J R et al 2008 Nanoscale magnetic sensing with an individual electronic spin in diamond *Nature* **455** 644–7
- [6] Balasubramanian G et al 2008 Nanoscale imaging magnetometry with diamond spins under ambient conditions *Nature* **455** 648–51
- [7] Hall L T, Cole J H, Hill C D and Hollenberg L C L 2009 Sensing of fluctuating nanoscale magnetic fields using nitrogen-vacancy centers in diamond *Phys. Rev. Lett.* **103** 220802
- [8] Cole J H and Hollenberg L C L 2009 Scanning quantum decoherence microscopy *Nanotechnology* **20** 495401
- [9] Hall L T, Hill C D, Cole J H and Hollenberg L C L 2010 Ultra-sensitive diamond magnetometry using optimal dynamic decoupling *Phys. Rev. B* **82** 045208
- [10] Fu C-C, Lee H-Y, Chen K, Lim T-S, Wu H-Y, Lin P-K, Wei P-K, Tsao P-H, Chang H-C and Fann W 2007 Characterization and application of single fluorescent nanodiamonds as cellular biomarkers *Proc. Natl Acad. Sci.* **104** 727–32
- [11] Chang Y-R et al 2008 Mass production and dynamic imaging of fluorescent nanodiamonds *Nat. Nanotechnology* **3** 284–8
- [12] Tisler J et al 2009 Fluorescence and spin properties of defects in single digit nanodiamonds *ACS Nano* **3** 1959–65
- [13] Gaebel T et al 2006 Room-temperature coherent coupling of single spins in diamond *Nat. Phys.* **2** 408
- [14] Dutt M V G, Childress L, Togan E, Jiang L, Maze J, Jelezko F, Zibrov A S, Hemmer P R and Lukin M D 2007 Quantum register based on individual electronic and nuclear spin qubits in diamond *Science* **316** 1312–6
- [15] Togan E et al 2010 Quantum entanglement between an optical photon and a solid-state spin qubit *Nature* **466** 730–4
- [16] Neumann P et al 2010 Quantum register based on coupled electron spins in a room-temperature solid *Nat. Phys.* **6** 249–53
- [17] Fuchs G D, Dobrovitski V V, Hanson R, Batra A, Weis C D, Schenkel T and Awschalom D D 2008 Excited-state spectroscopy using single-spin manipulation in diamond *Phys. Rev. Lett.* **101** 117601
- [18] Davies G and Hamer M F 1976 Optical studies of the 1.945 eV vibronic band in diamond *Proc. R. Soc. A* **348** 285–98
- [19] Loubser J H N and Van Wyk J A 1977 Optical spin-polarization in a triplet state in irradiated and annealed type 1b diamonds *Diam. Res.* **1** 11–15
- [20] Loubser J H N and van Wyk J A 1978 Electron spin resonance in the study of diamond *Rep. Prog. Phys.* **41** 1201
- [21] Reddy N R S, Manson N B and Krausz E R 1987 Two-laser spectral hole burning in a colour centre in diamond *J. Lumin.* **38** 46
- [22] van Oort E, Manson N B and Glasbeek M 1988 Optically detected spin coherence of the diamond N-V centre in its triplet ground state *J. Phys. C: Solid State Phys.* **21** 4385
- [23] Redman D A, Brown S, Sands R H and Rand S C 1991 Spin dynamics and electronic states of N-V centers in diamond by EPR and four-wave-mixing spectroscopy *Phys. Rev. Lett.* **67** 3420–3
- [24] Manson N B, Harrison J P and Sellars M J 2006 Nitrogen-vacancy center in diamond: model of the electronic structure and associated dynamics *Phys. Rev. B* **74** 104303
- [25] Rogers L J, Armstrong S, Sellars M J and Manson N B 2008 Infrared emission of the NV centre in diamond: zeeman and uniaxial stress studies *New J. Phys.* **10** 103024
- [26] Rogers L 2010 How far into the infrared can a colour centre in diamond emit? *Phys. Procedia* **3** 1557–61
- [27] Kaplyanskii A A 1964 Noncubic centers in cubic crystals and their piezospectroscopic investigation *Opt. Spectrosc.* **16** 329–37
- [28] Kaplyanskii A A 1964 Computation of deformation splitting of spectral transitions in cubic crystals *Opt. Spectrosc.* **16** 557–65
- [29] Hughes A E and Runciman W A 1967 Uniaxial stress splitting of doubly degenerate states of tetragonal and trigonal centres in cubic crystals *Proc. Phys. Soc.* **90** 827–38
- [30] Goss J P, Jones R, Breuer S J, Briddon P R and Öberg S 1996 The twelve-line 1.682 eV luminescence center in diamond and the vacancy-silicon complex *Phys. Rev. Lett.* **77** 3041–4
- [31] Manson N B and McMurtrie R L 2007 Issues concerning the nitrogen-vacancy center in diamond *J. Lumin.* **127** 98–103
- [32] Gali A, Fyta M and Kaxiras E 2008 Ab initio supercell calculations on nitrogen-vacancy center in diamond: electronic structure and hyperfine tensors *Phys. Rev. B* **77** 155206
- [33] Delaney P, Greer J C and Larsson J A 2010 Spin-polarization mechanisms of the nitrogen-vacancy center in diamond *Nano Lett.* **10** 610–4
- [34] Crowther P A and Dean P J 1967 Phonon interactions, piezo-optical properties and the inter-relationship of the n3 and n9 absorption-emission systems in diamond *J. Phys. Chem. Solids* **28** 1115–36
- [35] Davies G 1979 Dynamic Jahn–Teller distortions at trigonal optical centres in diamond *J. Phys. C: Solid State Phys.* **12** 2551–66

- [36] Manson N, Rogers L, Doherty M and Hollenberg L 2010 Optically induced spin polarisation of the NV- centre in diamond: role of electron-vibration interaction (arXiv:[1011.2840](https://arxiv.org/abs/1011.2840))
- [37] Doherty M W, Manson N B, Delaney P and Hollenberg L C L 2011 The negatively charged nitrogen-vacancy centre in diamond: the electronic solution *New J. Phys.* **13** 025019
- [38] Maze J R, Gali A, Togan E, Chu Y, Trifonov A, Kaxiras E and Lukin M D 2011 Properties of nitrogen-vacancy centers in diamond: the group theoretic approach *New J. Phys.* **13** 025025
- [39] Ham F S 1972 Jahn–Teller effects in electron paramagnetic resonance spectra *Electron Paramagnetic Resonance* ed S Geschwind (New York: Plenum) pp 1–119
- [40] Coulson C A and Kearsley M J 1957 Colour centres in irradiated diamonds: I. *Proc. R. Soc A* **241** 433–54
- [41] Lenev A and Rand S C 1996 Electronic structure of the N-V center in diamond: theory *Phys. Rev. B* **53** 13441–55
- [42] Manson N B, Beha K, Batalov A, Rogers L J, Doherty M W, Bratschitsch R and Leitenstorfer A 2013 Assignment of the NV⁰ 575 nm zero-phonon line in diamond to a ²E–²A₂ transition *Phys. Rev. B* **87** 155209
- [43] Jones R, Goss J P, Briddon P R and Öberg S 1997 N2 and N4 optical transitions in diamond: a breakdown of the vacancy model *Phys. Rev. B* **56** 1654–6